PHYSOR 2004-The Physics of Fuel Cycles and Advanced Nuclear Systems: Global Developments
Chicago, Illinois, April 25-29, 2004, on CD-ROM, American Nuclear Society, Lagrange Park, IL. (2004)

The Variational Nodal Method in *R-Z* Geometry

Hui Zhang & E. E. Lewis*
Northwestern University, Department of Mechanical Engineering, Evanston, IL 60208 USA

The variational nodal method contained in the Argonne National Laboratory code VARIANT is generalized to include *R-Z* geometry. Spherical harmonic trial functions are used in angle, and polynomials in space. The nodal volumes correspond to toroids, with rectangular cross sections, except along centerline where they are cylinders. The *R-Z* response matrix equations are solved using the iterative methods already contained in VARIANT. Results are given for both a one-group fixed source and a two-group eigenvalue problem.

KEYWORDS: Boltzmann Equation, R-Z Geometry, Neutron Transport, Nodal Method, Spherical Harmonics, Variational Method

1. Introduction

The variational nodal method has found substantial use in both diffusion theory and higher-order spherical harmonics approximations. It has been available in both two- and three-dimensional Cartesian and hexagonal geometries. However, the need sometimes arises for two-dimensional *R-Z* geometry calculations, particularly for scoping studies. The purpose of this work is to develop an *R-Z* option for the Argonne National Laboratory variational nodal code VARIANT [1, 2].

2. Theory

2.1 Variational Formulation

The variational nodal method is a primal hybrid finite element representation of the even-parity form of the transport equation. In the hybrid formulation, the problem domain V is decomposed into subdomains V_ν (also called elements or nodes):

$$V = \sum_\nu V_\nu . \tag{1}$$

Within each node, the even-parity form of the transport equation is solved in space ($\vec{r}$) and angle ($\hat{\Omega}$):

$$-\hat{\Omega}\cdot\vec{\nabla}\sigma^{-1}\hat{\Omega}\cdot\vec{\nabla}\psi^+(\vec{r},\hat{\Omega})+\sigma\ \psi^+(\vec{r},\hat{\Omega})=\sigma_s\int d\hat{\Omega}'\psi^+(\vec{r},\hat{\Omega}')+s(\vec{r}),\quad \vec{r}\in V_\nu \tag{2}$$

where ψ^+ is the even parity flux component, σ and σ_s the total and scattering cross sections and s the group source. The odd-parity flux ψ^-, which is related to ψ^+ by

* Corresponding author, Tel. 847-491-3579, FAX 847-491-3915, E-mail: e-lewis@northwestern.edu

$$\hat{\Omega}\cdot\vec{\nabla}\psi^{+}(\vec{r},\hat{\Omega})+\sigma\psi^{-}(\vec{r},\hat{\Omega})=0, \qquad \vec{r}\in\Gamma_{\nu} \tag{3}$$

is defined only along the node interface Γ_{ν} as a Lagrange multiplier.

The functional for the variational nodal method is given as a superposition of nodal contributions:

$$F[\psi^{+},\psi^{-}]=\sum_{\nu}F_{\nu}[\psi^{+},\psi^{-}], \tag{4}$$

where

$$F_{\nu}[\psi^{+},\psi^{-}]=\int_{\nu}dV\left\{\int d\Omega[\sigma^{-1}(\hat{\Omega}\cdot\vec{\nabla}\psi^{+})^{2}+\sigma\psi^{+2}]-\sigma_{s}\phi^{2}-2\phi s\right\}+2\int_{\nu}d\Gamma\int d\Omega\hat{\Omega}\cdot\hat{n}\psi^{+}\psi^{-}, \tag{5}$$

and ϕ is the scalar flux. This functional must be stationary with respect to arbitrary variations $\tilde{\psi}^{+}$ and $\tilde{\psi}^{-}$ about the true solutions ψ^{+} and ψ^{-}. Thus, we make the replacements $\psi^{+}\rightarrow\psi^{+}+\delta\tilde{\psi}^{+}$ and $\psi^{-}\rightarrow\psi^{-}+\varepsilon\tilde{\psi}^{-}$ where δ and ε are small positive constants, and require the linear terms in δ and ε to vanish. Setting the linear term in δ to zero yields the weak form of Eq. (2):

$$\int_{\nu}dV\int d\Omega[\sigma^{-1}(\hat{\Omega}\cdot\vec{\nabla}\tilde{\psi}^{+})(\hat{\Omega}\cdot\vec{\nabla}\psi^{+})+\tilde{\psi}^{+}(\sigma\psi^{+}-\sigma_{s}\phi-s)]+\int_{\nu}d\Gamma\int d\Omega\hat{\Omega}\cdot\hat{n}\tilde{\psi}^{+}\psi^{-}=0, \tag{6}$$

and applying the divergence theorem yields

$$\int_{\nu}dV\int d\Omega\tilde{\psi}^{+}(-\hat{\Omega}\cdot\vec{\nabla}\sigma^{-1}\hat{\Omega}\cdot\vec{\nabla}\psi^{+}+\sigma\psi^{+}-\sigma_{s}\phi-s)+\int_{\nu}d\Gamma\int d\Omega\hat{\Omega}\cdot\hat{n}\tilde{\psi}^{+}(\psi^{-}+\sigma^{-1}\hat{\Omega}\cdot\vec{\nabla}\psi^{+})=0. \tag{7}$$

Clearly, Eq. (2) must be satisfied if the volume integral is to vanish for arbitrary $\tilde{\psi}^{+}$, and Eq. (3) must be met at the interface for the surface integral to vanish. The continuity conditions across nodal interfaces may be stated as follows. Since the Lagrange multiplier ψ^{-} and its variation $\tilde{\psi}^{-}$ are uniquely defined at the interface, two conditions are imposed. First, the surface integral in Eq. (7) imposes continuity on $\sigma^{-1}\hat{\Omega}\cdot\vec{\nabla}\psi^{+}$. Second, requiring the linear term in ε to vanish yields for each nodal interface, say between nodes V_{ν} and $V_{\nu'}$, a condition of the form

$$\int_{\nu}d\Gamma\int d\Omega\hat{\Omega}\cdot\hat{n}\tilde{\psi}^{-}(\psi^{+}-\psi'^{+})=0, \tag{8}$$

since $\hat{n}_{\nu}=-\hat{n}_{\nu'}$. Thus ψ^{+} must be continuous across the interface.

2.2. Cylindrical Coordinates (r, z)

The *R-Z* cylindrical coordinates system is shown in Figure 1, together with an angular-direction coordinates system used to define the particle direction $\hat{\Omega}$. In this system, a spatial point is defined by its (r, z) coordinate and

$$\hat{\Omega} = \Omega_r \hat{r} + \Omega_\omega \hat{\omega} + \Omega_z \hat{z}, \tag{9}$$

where

$$\begin{aligned} \Omega_r &= (1-\mu^2)^{1/2} \cos\omega, \\ \Omega_\omega &= (1-\mu^2)^{1/2} \sin\omega, \\ \Omega_z &= \mu \end{aligned} \tag{10}$$

with $\mu = \cos\theta$. The $\hat{\Omega}\cdot\vec{\nabla}$ may be determined by [3, 4]

$$\hat{\Omega}\cdot\vec{\nabla} = \Omega_r \frac{\partial}{\partial r} - \frac{1}{r}\Omega_\omega \frac{\partial}{\partial \omega} + \Omega_z \frac{\partial}{\partial z}, \tag{11}$$

and the incremental angle is defined as $d\Omega = (4\pi)^{-1} d\mu d\omega$.

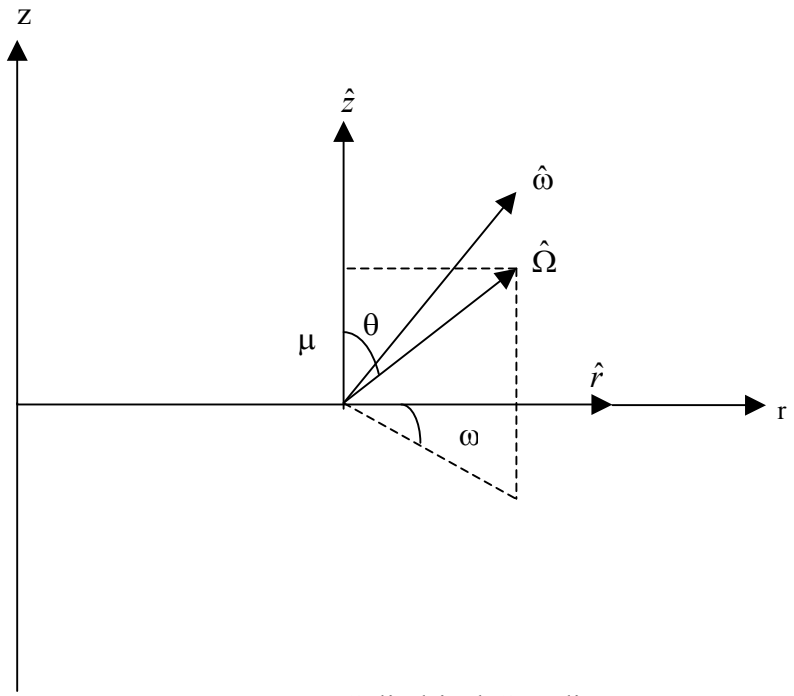

Fig. 1 Cylindrical Coordinates

2.3. Discretization

We begin by considering a rectangular node in *r, z* bounded on left and right by $r_l \le r \le r_r$ and on bottom and top by $z_b \le z \le z_t$ as shown in Figure 2. We expand the even-parity flux coefficients within the node as

$$\boldsymbol{\psi}^+(r,z,\hat{\Omega}) = \mathbf{g}^T(\hat{\Omega}) \otimes \mathbf{f}^T(r,z)\boldsymbol{\xi}_v. \qquad r_l \le r \le r_r, z_b \le z \le z_t \tag{12}$$

Here $\otimes$ denotes the Kronecker product, and $\mathbf{g}(\hat{\Omega})$ is vector of even-order spherical harmonics with M terms obey the orthonormal condition

$$\int d\Omega \mathbf{g}(\hat{\Omega})\mathbf{g}^T(\hat{\Omega}) = \mathbf{I}_M . \tag{13}$$

The spatial trial functions $\mathbf{f}(r,z)$ are complete polynomials. They are Legendre polynomials in z and also constructed to be orthogonal in r, so that

$$\frac{1}{V_v}\int_v dV \mathbf{f}(r,z)\mathbf{f}^T(r,z) = \mathbf{I}_I , \tag{14}$$

In R-Z geometry, $V_v = 2\pi(r_r^2 - r_l^2)(z_t - z_b)$ and

$$\int_v dV(\cdot) = 2\pi\int_{r_l}^{r_r} drr\int_{z_b}^{z_t} dz(\cdot) \tag{15}$$

The vector $\xi_\mathbf{v}$ in Eq, (12) contains the unknown coefficients.

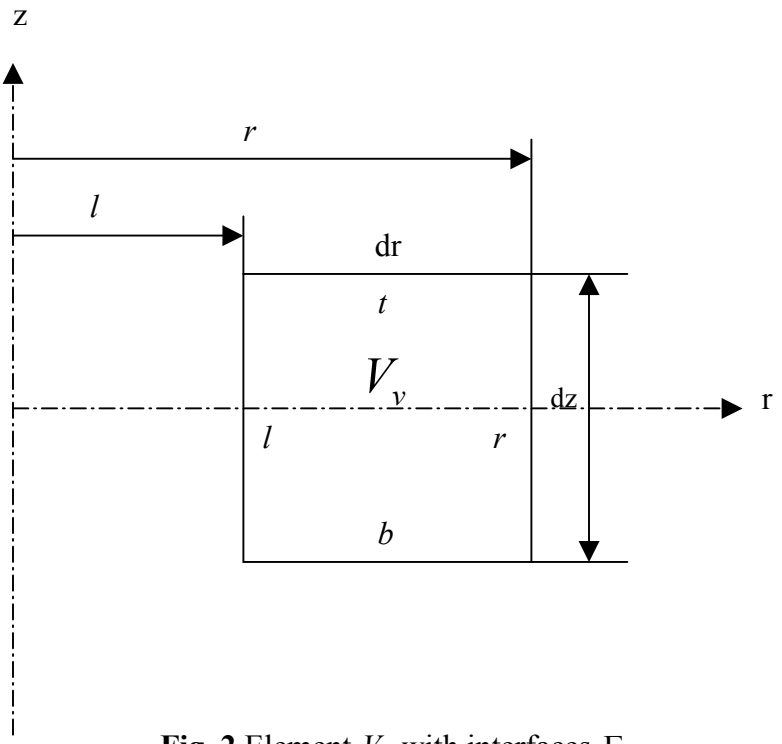

Fig. 2 Element V_v with interfaces Γ_v

Along the node interfaces, we make the expansions

$$\psi^-(\vec{r},\hat{\Omega}) = \mathbf{k}_\gamma^T(\hat{\Omega}) \otimes h_\gamma^T(z)\chi_\gamma^{'}, \qquad \vec{r} \in \Gamma_r, \Gamma_l$$

and (16)

$$\psi^-(\vec{r},\hat{\Omega}) = \mathbf{k}_\gamma^T(\hat{\Omega}) \otimes h_\gamma^T(z)\chi_\gamma^{'}, \qquad \vec{r} \in \Gamma_t, \Gamma_b$$

where $\mathbf{k}_\gamma(\hat{\Omega})$ is vector of odd-order spherical harmonics in which the angular coordinates have been rotated such that the polar angle, $\mu = \hat{\Omega} \cdot \hat{n}_\gamma$, is taken with respect to the surface normal. They obey the orthonormal conditions

$$\int d\Omega \mathbf{k}_\gamma(\hat{\Omega})\mathbf{k}_\gamma^T(\hat{\Omega}) = \mathbf{I}_N$$

and $\gamma = r,t,l,b$ (17)

$$\int d\Omega \mathbf{g}(\hat{\Omega})\mathbf{k}_\gamma^T(\hat{\Omega}) = \mathbf{0}$$

The spatial trial functions $\mathbf{h}_\gamma$ are set sets of orthogonal polynomials defined along the interfaces.

The source and the scalar flux may be approximated as

$$\mathbf{s} = \mathbf{w}s(r,z) \tag{18}$$

and $r_l \le r \le r_r, z_b \le z \le z_t$

$$\phi(\vec{r}) = \mathbf{w}^T \otimes \mathbf{f}^T(r,z)\boldsymbol{\xi}_\nu \tag{19}$$

with $[\mathbf{w}]_m = \delta_{m1}$.

The nodal volumes corresponding to the response matrices will be toroids with rectangular cross sections in the r, z plane. The central nodes, however, are cylinders with three surfaces. The centerline symmetry condition that

$$\lim_{r\to\infty} \psi^{\pm}(\vec{r},\hat{\Omega}) = \psi^{\pm}(z,\theta) \tag{20}$$

requires that the central nodes contain two sets of trial functions for ψ^+ and for ψ^- when spherical harmonics are employed. Only even functions in *r* are included in the spatial trial function sets for the Y_{l0} terms, which are independent of ω, causing the radial derivative vanishes at *r* = 0; only odd functions of *r* are included for the ω dependent Y_{lm}, $m \neq 0$ terms, causing them to vanish at the origin. With these stipulations, the singularities that would otherwise be encountered in applying the operator of Eq. (11) are removed. Note, also, that unlike Cartesian geometry, each response matrix in the radial direction is unique, even though the cross sections and the widths and heights of the nodes are same.

2.4. Response Matrix Evaluation

Response matrices are obtained from the foregoing space-angle trial functions by inserting them into Eqs. (4) and (5). This reduces the functional to the algebraic form:

$$F = \sum_{\nu} F_{\nu}[\zeta_{\nu}, \chi_{\nu}] \tag{21}$$

and

$$F_{\nu}[\zeta_{\nu}, \chi_{\nu}] = \zeta_{\nu}^{T}\mathbf{A}_{\nu}\zeta_{\nu} - 2\zeta_{\nu}^{T}\mathbf{s}_{\nu} + 2\zeta_{\nu}^{T}\mathbf{M}_{\nu}\chi_{\nu}. \tag{22}$$

The matrix $\mathbf{A_V}$ is given as

$$\mathbf{A}_{\nu} = \sigma_{\nu}^{-1}\mathbf{H}_{kk'} \otimes \int_{\nu} dV(\nabla_{k}\mathbf{f})(\nabla_{k'}\mathbf{f}^{T}) + (\sigma_{\nu}\mathbf{I}_{M} - \sigma_{s\nu}\mathbf{w}\mathbf{w}^{T}) \otimes V_{\nu}\mathbf{I}_{I}, \tag{23}$$

where repeated subscripts k or k' indicates summation with $k, k' = r, \omega, z$, and

$$\begin{aligned} \nabla_{r}\mathbf{f} &= \partial\mathbf{f}/\partial r, \\ \nabla_{\omega}\mathbf{f} &= \mathbf{f}/r, \\ \nabla_{z}\mathbf{f} &= \partial\mathbf{f}/\partial z. \end{aligned} \tag{24}$$

The incremental spatial volume is given by $dV = 2\pi r dr dz$.

Each of the elements of $\mathbf{A_V}$ is given in terms of integrals over known spatial or angular trial functions:

$$\mathbf{H}_{kk'} = \int d\Omega \Omega_{k}\Omega_{k'}\breve{\mathbf{g}}_{k}\breve{\mathbf{g}}_{k'}^{T}, \tag{25}$$

where

$$\begin{aligned} \breve{\mathbf{g}}_{r,z} &= \mathbf{g}, \\ \breve{\mathbf{g}}_{\omega} &= -\partial\mathbf{g}/\partial\omega. \end{aligned} \tag{26}$$

The source is

$$\mathbf{s}_{\nu} = \int_{\nu} dV \mathbf{s} \otimes \mathbf{f}. \tag{27}$$

The surface coefficients are partitioned according to the four interfaces:

$$\chi_{\nu} = \begin{bmatrix} \chi_{r}' \\ \chi_{t}' \\ \chi_{l}' \\ \chi_{b}' \end{bmatrix} \tag{28}$$

The $\mathbf{M}_{\nu}$ matrix is then given as

$$\mathbf{M}_{\nu} = \left[\mathbf{M}_{r}', \mathbf{M}_{t}', \mathbf{M}_{l}', \mathbf{M}_{b}'\right], \tag{29}$$

$$\mathbf{M}_{\gamma}' = \mathbf{E}_{\gamma} \otimes \mathbf{D}_{\gamma}, \qquad \gamma = r,t,l,b \tag{30}$$

where

$$\vec{\mathbf{E}}_{\gamma} = \int d\Omega \hat{\Omega} \cdot \hat{n}_{\gamma}\mathbf{g}(\hat{\Omega})\mathbf{k}_{\gamma}^{T}(\hat{\Omega}), \tag{31}$$

and

$$\mathbf{D}_\gamma = 2\pi r_\gamma \int_{z_b}^{z_t} dz \mathbf{f}(r_\gamma, z)\mathbf{h}_\gamma^T(z), \qquad \gamma = r,l$$
$$\mathbf{D}_\gamma = 2\pi \int_{r_l}^{r_r} dr r \mathbf{f}(r, z_\gamma)\mathbf{h}_\gamma^T(r). \qquad \gamma = t,b \tag{32}$$

We may now obtain a set of algebraic equations by requiring the discretized functional to be stationary. To examine arbitrary variations about the solutions, we make the replacements $\boldsymbol{\zeta}_\nu \to \boldsymbol{\zeta}_\nu + \delta\tilde{\boldsymbol{\zeta}}_\nu$ and $\boldsymbol{\chi}_\nu \to \boldsymbol{\chi}_\nu + \delta\tilde{\boldsymbol{\chi}}_\nu$ in Eqs. (21) and (22). Requiring the linear term in δ to vanish yields

$$\mathbf{A}_\nu \boldsymbol{\zeta}_\nu + \mathbf{M}_\nu \boldsymbol{\chi}_\nu = \mathbf{s}_\nu. \tag{33}$$

Requiring the linear term in ε to vanish imposes continuity across nodal interfaces of the moments defined by

$$\boldsymbol{\psi}_\nu = \mathbf{M}_\nu^T \boldsymbol{\zeta}_\nu. \tag{34}$$

We may solve Eq. (33) for $\boldsymbol{\zeta}_\nu$,

$$\boldsymbol{\zeta}_\nu = \mathbf{A}_\nu^{-1}\mathbf{s}_\nu - \mathbf{A}_\nu^{-1}\mathbf{M}_\nu \boldsymbol{\chi}_\nu, \tag{35}$$

and combine the result with Eq. (34) to obtain

$$\boldsymbol{\psi}_\nu = \mathbf{M}_\nu^T \mathbf{A}_\nu^{-1}\mathbf{s}_\nu - \mathbf{M}_\nu^T \mathbf{A}_\nu^{-1}\mathbf{M}_\nu \boldsymbol{\chi}_\nu. \tag{36}$$

At this point, we have written the even-parity flux moments $\boldsymbol{\psi}_\nu$ at the node interface in terms of the source and the odd-parity interface moments $\boldsymbol{\chi}_\nu$, while imposing the continuity of both of these moments between neighboring nodes. The final step is to transform variables such that Eq. (36) may be written in terms of a response matrix. Introducing the partial current-like variables

$$\mathbf{j}_\nu^\pm = \tfrac{1}{4}\boldsymbol{\psi}_\nu \pm \tfrac{1}{2}\boldsymbol{\chi}_\nu \tag{37}$$

into Eq. (39) and (40) then yields response matrix equation for each node:

$$\mathbf{j}_\nu^+ = \mathbf{R}_\nu \mathbf{j}_\nu^- + \mathbf{B}_\nu \mathbf{s}_\nu, \tag{38}$$

where $\mathbf{R}_\nu = \left(\tfrac{1}{2}\mathbf{M}_\nu^T \mathbf{A}_\nu^{-1}\mathbf{M}_\nu + \mathbf{I}\right)^{-1}\left(\tfrac{1}{2}\mathbf{M}_\nu^T \mathbf{A}_\nu^{-1}\mathbf{M}_\nu - \mathbf{I}\right)$ and $\mathbf{B}_\nu = \left(\tfrac{1}{2}\mathbf{M}_\nu^T \mathbf{A}_\nu^{-1}\mathbf{M}_\nu + \mathbf{I}\right)^{-1} \tfrac{1}{2}\mathbf{M}_\nu^T \mathbf{A}_\nu^{-1}$.

3. Results

The *R-Z* formalism is being implemented as a modification of the multigroup VARIANT code at Argonne National Laboratory, for both diffusion theory and higher-order spherical harmonics

calculations. Both fixed source and eigenvalue options are included. To test the fixed source capability the well-known Iron-water problem [5] has been recast from *X-Y* to *R-Z* geometry, with all dimensions and cross sections remaining the same. Figures 3 and 4 show P_1 and P_3 results close to the vacuum boundaries. Fine meshes with $\Delta r = \Delta z = 1$ cm, and a coarse mesh, with $\Delta r = \Delta z = 3$ cm, are presented. For comparison, fine mesh x-y calculations are also included. The substantial transport effects are, as expected, present in *R-Z* as well as *X-Y* geometry.

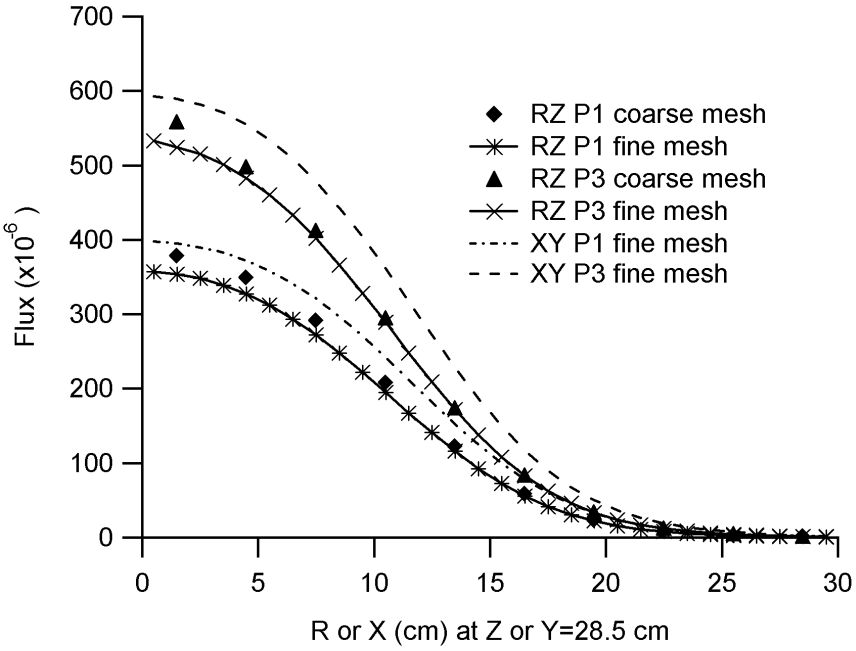

Fig. 3 Flux distribution close to the vacuum boundary on the top for the Iron-water problem

To examine spatial truncation errors, we utilize two-group eigenvalue problems. Table 1 provides P_1 eigenvalue results using two group MOX fuel and water cross sections. The core is 40 cm in radius and 80 cm in height surrounded by radial and axial reflectors 20 cm thick. A reflected boundary condition is used to reduce the modeling to the upper half of the core. The eigenvalue is tabulated vs. both *h* and *p* refinement. Aside from the coarsest nodes, the accuracy increases faster with *p* refinement (i.e. increasing the polynomial order in the interface approximation) than in reducing the mesh size in *h* refinement. Moreover, both CPU time and memory requirements increase substantially with mesh size reduction, but much less so with increased polynomial order.

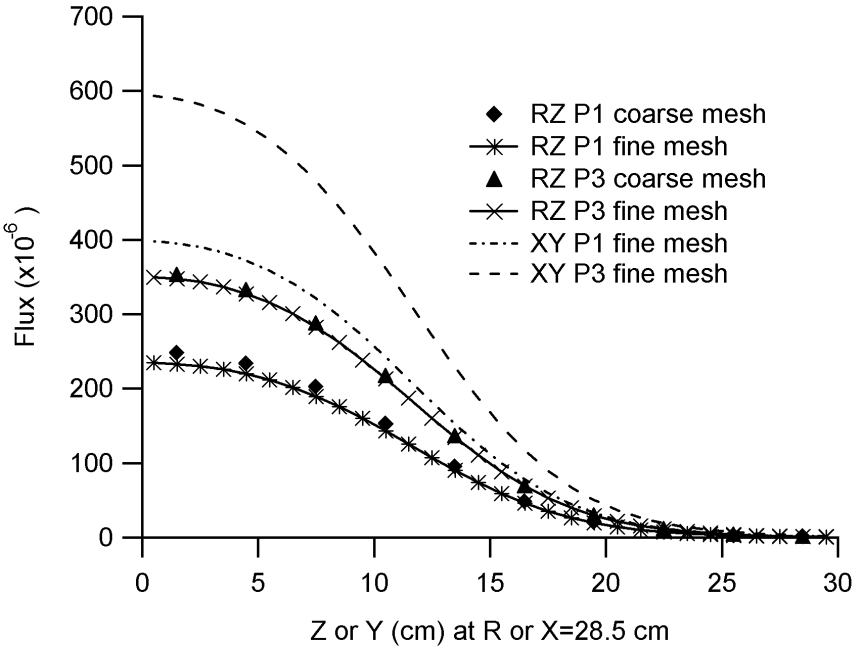

Fig. 4 Flux distribution close to the vacuum boundary on the right for the Iron-water problem

Interface / Δr & Δz	Flat	Linear	Quadratic
10cm	0.95450 (1.21×10^{-1}%)	0.95349 (1.47×10^{-2}%)	0.95349 (1.47×10^{-2}%)
4cm	0.95351 (1.68×10^{-2}%)	0.95335 (0.00%)	0.95335 (0.00%)
2cm	0.95339 (3.15×10^{-3}%)	0.95335 (0.00%)	0.95335 (0.00%)
1cm	0.95336 (1.05×10^{-3}%)	0.95335 (0.00%)	0.95335 (0.00%)

Table 1 Comparison of *h*-refinement and *p*-refinement for Two-Region Eigenvalue Problem

4. Conclusions

The foregoing results demonstrate the ability of the variational nodal method to treat problems in R-Z geometry. The curvilinear coordinate system, however, presents two challenges that are not present in Cartesian geometry. First, the central elements must be treated specifically, and the trial functions constrained to assure that the appropriate symmetry conditions on the angular flux are met along the center line. Second, each radial response matrix must be calculated separately, for there is no

translational invariance in the radial direction; each radial node corresponds to a toroid with a unique radius.

Acknowledgements

This work was supported, in part, through Department of Energy contracts DE-FG07-01: ID14106 & ID14108.

References

1. G. Palmiotti, E. E. Lewis & C. B. Carrico, "VARIANT: VARIational Anisotropic Nodal Transport for Multidimensional Cartesian and Hexagonal Geometry Calculation," Argonne National Laboratory ANL-95/40, 1995.
2. E. E. Lewis, C. B. Carrico and G. Palmiotti, "Variational Nodal Formulation for the Spherical Harmonics Equations," Nucl. Sci. Eng., 122, 194-203, 1996
3. R. Douglas O'Dell and Raymond E. Alcouffe, "Transport Calculation for Nuclear Analyses: Theory and Guidelines for Effective Use of Transport Codes," Los Alamos National Laboratory LA-10983-MS, 1987
4. E. E. Lewis and W. F. Miller, Jr., "Computational Methods of Neutron Transport," John Wiley & Sons, New York, 1984
5. E. M. Gelbard, "Argonne Code Center: Benchmark Problem Book," ANL-7416 Supplement 1 Mathematics and Computers, Argonne National Laboratory, 1972